Development and validation of a comprehensive 1-D model to simulate gas hold-up and gas–liquid transfer in deep air–water bubble columns

Timo Larsson, Camilo Duran Quintero, Sylvie Gillot, Arnaud Cockx, Yannick Fayolle

Development and validation of a comprehensive 1-D model to simulate gas hold-up and gas–liquid transfer in deep air-water bubble columns

T. Larsson[a], C. Duran Quintero[b], S. Gillot[c], A. Cockx[d] Y. Fayolle[a]

[a] Université Paris-Saclay, INRAE, UR PROSE, 1 rue Pierre-Gilles de Gennes, Antony, F-92761, France

[b] Université de Nantes, GEPEA, UMR 6144, 37 bd. de l'Université, F-44600, Saint Nazaire, France

[c] INRAE, REVERSAAL, 5 Rue de la Doua, Villeurbanne Cedex, F-69625, France

[d] TBI, Université de Toulouse, CNRS, INP, INSA, UPS, Toulouse, France

Abstract

This study proposed to develop a model coupling hydrodynamics and mass transfer in order to gain an understanding of measurements taken on air-water bubble columns with low gas hold-up. Three experimental datasets with various operating conditions (water quality, liquid height, air flow range) were chosen. The model analyzes and interprets the significant impact of the local hydrostatic pressure and the effects of contamination on hydrodynamic and mass transfer parameters. The oxygen concentration in gas significantly depletes with the distance from diffusers, which explains the difference between the calculated mean of the local $<k_La>$ and global K_La coefficients. This difference is highly significant for a high bubble column and/or systems with a low mean bubble size. The impact of water quality on mass transfer can be characterized by the contamination angle using comprehensive 1-D modeling and highlights a differentiated impact on the hydrodynamic or mass transfer parameters.

Keywords

1D Model, Oxygen mass transfer, Aeration, Wastewater treatment, Bubble column

1. Introduction

In the domain of water and wastewater treatment and recovery, gas–liquid reactors are often used to perform gas–liquid oxygen mass transfer. In particular, air bubbles are injected in aeration tanks to provide microorganisms with the oxygen they require for their growth. Aeration systems in these processes must be efficient in terms of mass transfer coefficients, easy to construct, with no moving parts and a low pressure drop through the air diffusers (Manjrekar 2016). In this study, an analogy is made between bubble columns and wastewater aeration tanks, since they can both operate in the bubbly flow regime with similar heights and gas hold-up ranges. Indeed, using a deep bubble column allows one to reproduce the water heights and gas–liquid contact times encountered in aeration tanks (Gillot and Héduit 2008, Duran et al. 2016, Baeten et al. 2020). Similarly, air flowrates can be set to obtain gas superficial velocities and gas hold-ups ranges used in aeration tanks (Shah et al. 1982, Duran et al. 2016, Amaral et al. 2018). This analogy aims at helping reach a better understanding of fundamental phenomena that affects gas–liquid mass transfer in the bubbly flow regime, in order to optimize the aeration systems that remain the main energy consumer in water resource recovery facilities (Rosso and Stenstrom 2005, Longo et al. 2016).

For systems with low gas hold-ups (< 5%) and fine bubble diffusers, air bubbles are spherical or ellipsoidal with few coalescence and break-up phenomena (Talvy et al. 2007a, Colombet et al. 2015). However, bubble coalescence is more likely to occur in systems with denser bubble swarms and higher gas hold-ups and bubble diameters. In an air–water bubble column with fine bubble diffusers, the homogeneous flow regime without coalescence can be maintained under a transitional gas superficial velocity between 0.04 and 0.08 m/s (Mudde et al. 2009). In Besagni et al. (2016), the coarse gas sparger used led to an early disruption of the bubbly flow due to both non-uniform distribution and changes in bubble size generation. Loubière et al. (2003) also pointed out that bubble size variation depended upon the type of diffuser with a flexible porous membrane, the initial bubble size increases as the superficial gas velocity rises, whereas when using a rigid orifice, bubble size varies slightly depending on superficial gas velocity.

In air-water systems, the effect of bubble contamination on mass transfer is another frequently observed process and is mainly due to surfactants (Pöpel and Wagner 1994; Capela et al. 2002; Sardeing et al. 2006, Rosso et al. 2006, Jimenez et al. 2014) as well as aqueous salt solutions such as in biological media (Zlokarnik 2005). Contaminated bubbles yield lower mass transfer coefficients than perfectly clean bubbles, even though the level of bubble contamination may be difficult to quantify (Sardeing et al. 2006, Xu et al. 2018).

Water height also has an impact on overall mass transfer (Deckwer et al. 1974, Giovannettone and Gulliver 2008) since the gradients of the gas–phase composition and pressure appear to have highly interactive non-linear effects (Baeten at al. 2020). First, bubble diameter varies with hydrostatic pressure (Capela et al. 2002, Giovanettonne et al. 2009, Fayolle et al. 2010, Amaral et al. 2018), which has an influence on the gas–liquid interfacial area. In addition, the oxygen saturation concentration varies depending upon column height (Rubio et al. 1999) and the dissolved oxygen concentration profile at steady state can be very pronounced, suggesting local variation of the transfer rate even if the overall net transfer of oxygen is close to zero (Giovannettone and Gulliver 2008). The combination of these phenomena induce oxygen depletion in air bubbles, essentially explained by competition between the transfer rate and bubble convection (Talvy et al. 2007a, Giovanettonne and Gulliver 2008, Baeten et al. 2020).

To provide a comprehensive description of gas transfer inside deep air-water bubble columns, the classical one-dimensional two-fluid model **(**Wallis 1969, Cockx et al. 1997, Camacho-Rubio at al. 2001, Vitankar and Joshi 2002) developed in previous studies for airlift reactors, aeration tanks or bubble columns has been extended (Talvy et al. 2007a, Talvy et al. 2007b, Colombet et al. 2013). Since the transfer rate gradient increases with the height of the bubble column via the various well-identified mechanisms discussed above, all these phenomena need to be combined in a new model structure where both hydrodynamics and mass transfer are solved together to consider the effect of pressure and gas depletion.

One-dimensional (1-D) models are simple but rigorous and appear to be relevant when applied to bubble columns since gas flows are mainly in the vertical axis. Most existing models consider a constant superficial gas velocity since they apply to low height columns (Talvy 2007b, Colombet et al. 2013) and thus the pressure effect can be ignored. However, this may not be the case for columns with a high liquid height, as shown in studies taking the effect of pressure on gas solubility into account (Dhaoudi et al. 2008), or both gas solubility and gas flowrate (Giovanettone and Gulliver 2008, Baeten et al., 2020). In these investigations, the overall mass transfer coefficient K_La was considered, even though representing hydrodynamic variations together with changes in mass transfer (separating k_L from a) would be more useful to better interpret experimental results. In this context, the aim of this study was to develop a model that couples hydrodynamics and mass transfer in order to gain an understanding of measurement results obtained on systems with low gas hold-up under different configurations. Based on a literature review, the correlations that can be used to represent hydrodynamic and mass transfer phenomena (drag coefficient, mass transfer coefficient, collective bubble effects due to high gas hold-up) were identified. The simulation results were compared to observed data obtained in three experimental setups showing contrasting operating conditions (in terms of water height, gas hold-up, bubble diameter and interface contamination). Their specific relevant hydrodynamic and oxygen transfer phenomena were analyzed by modeling and simulation. To begin, after presenting the experimental datasets, the different processes considered in the comprehensive model are described. Subsequently, the simulated results are compared with the experimental data to choose between the different options concerning the model structure (closure relations) and to interpret the experimental results obtained under varied operating conditions.

2. Material and methods

The proposed 1-D model is used to investigate the results extracted from three experimental datasets obtained in clear water (Colombet et al. 2015, Duran et al. 2016, Amaral et al. 2018).

2.1 Experimental datasets

The database is composed of three experimental datasets obtained in bubble columns showing a low gas hold-up (less than 6%). They were selected because of their wide range of operating conditions (superficial gas velocity and gas hold-up) and the availability of data. Table 1 presents the main operating conditions for the three experimental datasets.

Table 1. Experimental conditions for the bubble column datasets

Dataset	Continuous fluid phase	Bubble sparger type	H_L (m)	d_B expressed at P_{atm} ($\times 10^{-3}$m)	j_g at P_{atm} ($\times 10^{-3}$m/s)	ε_g (%)	Reference
D1	Tap water	EPDM membrane	1.30	1.5 - 1.8	0.3 - 1.2	0.1 - 0.4	Amaral et al. (2018)
D2	Tap water	EPDM membrane	4.40	3.0 - 4.0	2.0 - 4.5	0.5 - 1.5	Duran et al. (2016)
D3	Filtered tap water	Capillaries	0.76	2.3 - 3.4	2.0 - 15.5	0.5 - 6.0	Colombet et al. (2015)

With : d_B mean bubble diameter, P_{atm} standard atmospheric pressure (1013 hPa), j_g superficial gas velocity, ε_g overall gas hold-up, H_L liquid height.

The water quality slightly differed from one dataset to another. In particular, the liquid used in Dataset D3 was filtered tap water (15 µm cutoff threshold) and tap water for D1 and D2.

Datasets D1 and D2 were obtained in bubble columns equipped with EPDM membrane diffusers, similar to the ones installed in full-scale aeration tanks. For Dataset D1, the water height was quite low (1.30 m). The superficial gas velocity and associated mean bubble size and gas hold-up were significantly lower in comparison to the other datasets. Dataset D2 corresponds to the experimental bubble column with the highest liquid height (4.5 m) in the lower range of liquid heights found in industrial aeration tanks, which allows for the study of the impact of hydrostatic pressure on hydrodynamics and mass transfer phenomena. A more complete description of this experimental dataset is provided in the following section, given that clear water results are not fully described in the published article (Duran et al. 2016).

Figure 1 presents hydrodynamic and mass transfer characteristics as a function of the superficial gas velocity for Dataset D2.

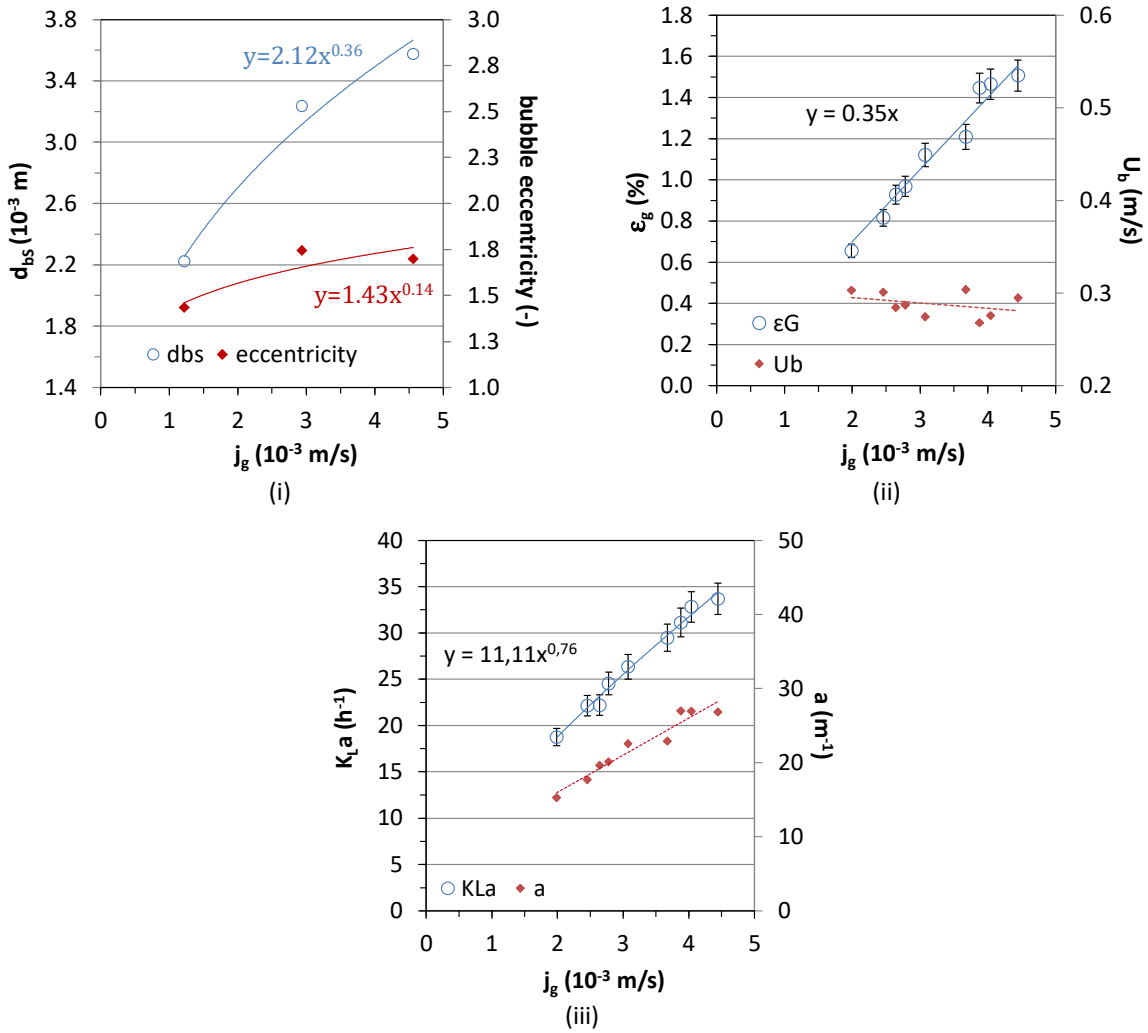

Figure 1. (i) Mean bubble Sauter diameter and mean bubble eccentricity measured at 1 m in height from the diffuser, (ii) overall gas hold-up (ε_g) and mean bubble rise velocity (U_b) at 20°C, (iii) overall oxygen transfer coefficient K_La expressed at 20°C and gas–liquid interfacial area (a) as a function of the superficial gas velocity – dataset D2

The mean bubble Sauter diameter increased from 2.2 to 3.6 mm with an increase in the superficial gas velocity (j_g) from 1.2 to 4.6 mm/s. The effect of the airflow rate on bubble size was more significant at lower superficial gas velocities because the membrane stretches and the pore size increases under the effect of the pressure associated with the airflow rate. Concerning the bubbles'

shape, their eccentricity slightly increased from 1.4 to 1.7 with the increase of the superficial gas velocity. Classically, the overall gas hold-up is a linear function of the superficial gas velocity, whereas the oxygen transfer coefficient follows a power law. The mean bubble rise velocity deduced ($U_b=j_g/\varepsilon_g$, for homogeneous distribution of gas along the column's surface) slightly decreased as the superficial air velocity increased. The reduction of U_b can be attributed to the collective effects (the interaction between bubbles) that ended up with higher bubble drag coefficients, as explained by Colombet et al. (2011). Since the estimated K_L coefficient ($K_L=K_La/a$) remains almost constant within the range of the j_g studied, the increase in the overall oxygen transfer coefficient (K_La) is mainly related to the increase in the interfacial area (estimated form d_{bs}, ε_g and bubble eccentricity; see Eq. 30 below).

Dataset D3 includes a wide range of superficial gas velocities and gas hold-up, even though the water height is lower in comparison with the other datasets. The bubble injection system consists of a network of stainless steel capillaries (with an inner diameter of 0.2 mm), that makes it possible to obtain a homogeneous bubble swarm. In contrast, the diffuser of the two other datasets, a porous EPDM membrane, provides a more heterogeneous initial bubble size distribution as commonly found in water treatment. In order to focus on low gas hold-up systems, the data considered were limited to gas hold-up lower than 6%, despite the wider range in the complete study (Colombet et al. 2013).

On the basis of transfer numbers (N_T), these datasets were compared with different previous databases from lab-scale (Capela et al., 2002) to full-scale aeration tanks (Fayolle et al. 2010, Fayolle et al. 2011). This dimensionless group ($N_T = \frac{K_L a_{20}}{j_g}\left(\frac{{\mu_L}^2}{{\rho_L}^2 g}\right)^{1/3}$) defined by Zlokarnik (1979) and Roustan (1996) has the same physical meaning as the specific standard oxygen transfer efficiency (SSOTE in %) per meter of diffuser submergence for clear water operating conditions (Gillot et al. 2005). Figure 2 presents the transfer number as a function of the mean Sauter bubble diameter for the different databases selected and datasets D1–D3.

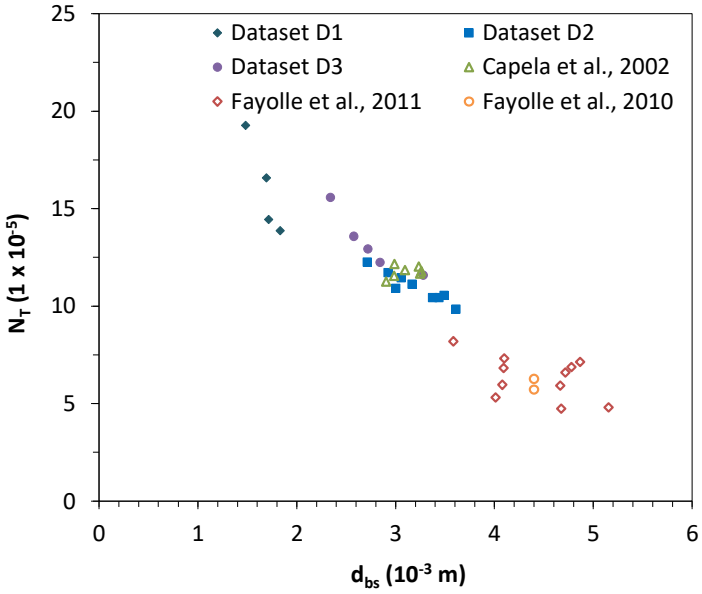

160

161 **Figure 2.** Transfer number (N_T) versus bubble Sauter diameter for selected databases (lab-scale [Capela et al.,
162 2002] and full-scale [Fayolle et al., 2010 and 2011]) and datasets 1–3.

163 For reactors with different configurations (from pilot scale to full-scale reactors), the transfer number
164 (N_T) seemed to be determined by the Sauter diameter, which fixes the bubble surface mobility and
165 the G-L interfacial area by controlling the overall gas hold-up. The results also clearly demonstrate
166 that the transfer number is an adequate scale-up factor for systems equipped with fine bubble
167 diffusers. Likewise, through the comparison with data obtained at full-scale, these results validate
168 the representativeness of the three datasets in terms of mass transfer mechanisms.

169

170 2.2. Two-Phase One-Dimensional Model

171 The proposed model is a 1-D model derived for low soluble gas mass transfer into a liquid in deep
172 bubble columns, applied to an air–water system (O_2 is considered to be the only gas transferred).
173 Since the calculated variables are homogenous and evenly distributed along the cross section, a 1-D
174 approach can be considered. The model first calculates hydrodynamic variables (gas hold-up,
175 changes in bubble diameter, gas velocity) considering steady-state conditions. Then, hydrodynamic
176 results are used as input values to calculate the transient oxygen mass transfer from the gas phase to

177 the liquid phase. The impact of the oxygen transfer on the bubble size and associated hydrodynamics
178 is ignored.
179 Contrary to other existing 1-D models (Giovannettonne and Gulliver, 2008, Baeten et al. 2020), the
180 impact of pressure on gas superficial velocity and bubble diameter is taken into account and its
181 impact on gas hold-up and mass transfer is fully considered and analyzed. The model is based on a
182 simplified Eulerian two-fluid model such as reported in Talvy et al. (2007a,b), where mass balance for
183 the gas and liquid phases and momentum interactions between the two phases are considered. The
184 proposed model implies different hypotheses related to the considered system (oxygen transfer in
185 batch air-water bubble column with low gas hold-up): (i) the impact of the mass transfer on the
186 bubble size and associated hydrodynamics is neglected, (ii) no vertical liquid flow is considered, (iii)
187 the bubbly flow is homogeneously distributed along the cross-section of the bubble column and (iv)
188 coalescence is neglected. The column is discretized along its height (50 layers along z), so the
189 variables are calculated locally at each discretization point.
190 Table 2 summarizes the values considered for the fluid properties and the main parameters of the
191 model (T = 20°C and P_{ref} = 1 atm).
192
193 **Table 2. Physico-chemical properties of the system (T = 20°C and P_{ref} = 1 atm)**

Parameter	Value	Unit
Water density, ρ_L	998.2	kg/m^3
Water dynamic viscosity, μ_L	1.10^{-3}	Pa.s
Water surface tension, σ	73	mN/m
Air density, ρ_G	1.2	kg/m^3
Oxygen diffusivity in water, D	2.10^{-9}	m^2/s
Gravity constant, g	9.81	m/s^2
Temperature, T	20	°C
Atmospheric pressure, (P_{ref})	1	atm

194
195 2.2.1. Equation of the 1-D model
196 All variables were averaged along each cross section of the column in order to provide a simple 1-D
197 model. As an example, the local gas hold-up in a cross-section S is given in Eq.1 (Talvy et al., 2007b).

$$\varepsilon_k = <\alpha_k> = \frac{1}{S}\iint_A \alpha_k dS \quad \text{(Eq. 1)}$$

where ε_k is the mean gas hold-up in the section, and α_k is the local gas hold-up at a specific point in the section. For the velocities, only the averaged axial components are different from zero and velocity vectors are thus reduced to scalars in the following.

2.2.2. Model structure: steady state hydrodynamic calculation

The hydrodynamic equations solved in the model are presented in the following sections.

2.2.2.1 Mass and flow rate conservation equation

The mass balance equation in a diphasic system is written as follows (Talvy et al. 2007a):

$$\frac{\partial \alpha_k \rho_k}{\partial t} + \nabla \alpha_k \rho_k \overline{U_k} = \overline{m_K} \quad \text{(Eq. 2)}$$

where α_k is the volume fraction, ρ_k the density and $\overline{U_k}$ the average velocity of phase k, which stands for gas (g) or liquid (l). The first term on the left side corresponds to mass variation over time in phase k, the second to mass transport by advection in the phase k, and the term on the right side ($\overline{m_K}$) corresponds to a statistical average mass transfer between the two phases.

In a 1-D system, Eq.2 becomes:

$$\frac{\partial(\varepsilon_k \rho_k)}{\partial t} + \frac{\partial}{\partial z}(\varepsilon_k \rho_k U_{kz}) = < m_k > \quad \text{(Eq. 3)}$$

With a steady state flow and assuming that average mass transfer between phases implied in the mass balance is ignored, the equation becomes for the liquid and the gas, respectively:

$$\varepsilon_l \rho_l U_l = Cst = \rho_l \frac{Q_l}{S} = \rho_l j_l \quad \text{(Eq. 4)}$$

$$\varepsilon_g \rho_g U_g = Cst = \rho_g \frac{Q_g}{S} = \rho_g j_g \quad \text{(Eq. 5)}$$

where Q_k and j_K are the flow rate and the superficial velocity (m/s), respectively, of phase k.

If it is considered that there is no liquid flow (j_l= 0, as in a batch bubble column), only the equation for the gas phase remains and the previous equation becomes:

$$\varepsilon_g = \frac{j_g}{U_g} \quad \text{(Eq. 6)}$$

since the sum of the different phase volume fractions is equal to unity:

$$\varepsilon_l = 1 - \varepsilon_g \quad \text{(Eq. 7)}$$

2.2.2.2 Gas velocity equation: the Zuber and Findlay drift flux model

Zuber and Findlay (1965) proposed the following interfacial momentum transfer model:

$$U_g = C_0\, j + G = C_0\left(j_g + j_l\right) + G \quad \text{(Eq. 8)}$$

Gas velocity (U_g) has two components, the first one corresponds to the gas transport resulting from mixing (induced by mixture velocity j composed of gas and liquid superficial velocity, j_g and j_l respectively) and the second one is gas slip velocity G, which corresponds to gas transport due to buoyancy. The latter will be further developed below. The drift-flux coefficient (C_0) is related to the non-uniformity of the gas-liquid flow field in the cross section and can be estimated from computational fluid dynamics (CFD) simulations, as in Talvy et al. (2005). However in the case of a homogeneous flow it can be considered close to 1. On the other hand, its extreme value would be 1.5 in the case of a spatially heterogeneous bubbly flow (Talvy et al. 2005).

With a homogeneous flow (C_0 = 1) and without the liquid flow rate (j_L = 0), the previous equation becomes:

$$U_g = j_g + G \quad \text{(Eq. 9)}$$

For homogeneous bubble columns at a low gas flow rate, $j_g << G$ and then the gas velocity U_g is finally assumed equal to the bubble slip velocity G.

Note that when the drift flux coefficient C_0 is equal to 1, radial gas fraction profiles are not considered and thus radial interfacial forces as lift and turbulent dispersion are neglected for the axial resolution (Talvy et *al.*, 2007a, b).

2.2.2.3 Gas slip velocity equation

A force balance applied to a rising gas bubble in a quiescent liquid and at steady state where the bubble has reached its terminal rising velocity consists in equilibrium between buoyancy and drag forces. The added mass force can be neglected in 1D models after a very short distance from the bubble sparger, when the fully developed gas velocity is established (Talvy et *al.*, 2007a, Colombet et *al.*, 2013).Thus, after simplification, the slip velocity G between the two phases can be calculated using Eq. 10 (Talvy et al. 2007b):

$$G = \sqrt{\frac{4}{3}\frac{{d_v}^3}{d_p^2}\frac{(\rho_l - \rho_g)}{\rho_l}\frac{g}{C_D}} \quad \text{(Eq. 10)}$$

with g the gravity constant (9.81 m/s^2), d_V the volume equivalent bubble diameter (m), C_D the drag coefficient (-), and d_p the surface equivalent bubble diameter (m).

Furthermore, if the two equivalent diameters are considered equals ($d_v = d_p = d_B$, for a spherical bubble, for example) and if gas density is ignored in comparison with liquid density, the following simplified equation is obtained:

$$G = \sqrt{\frac{4}{3} d_B \frac{g}{C_D}} \quad \text{(Eq. 11)}$$

2.2.2.4 Drag coefficient equation

Several correlations to calculate the drag coefficient exist in the literature, mostly expressed through dimensionless numbers. In the case of a single rigid particle, the following law involving the Reynolds number can be applied (Schiller and Naumann 1938):

$$C_D = \begin{cases} \frac{24}{Re} * (1 + 0.15\, Re^{0.687}) \; for \; Re < 1000 \\ 0.44 \; for \; Re > 1000 \end{cases} \quad \text{(Eq. 12)}$$

255 However, even though this correlation is often used for rigid spherical bubbles, it is not suitable for
256 oblate ellipsoidal bubbles where the eccentricity effect drastically affects the drag coefficient (Talvy
257 et al. 2007b).
258 With ellipsoidal bubbles, when the surface tension effects are significant, drag laws based on the
259 Eötvös number are more relevant (Tomiyama et al. 1998, Dijkhuizen et al. 2010). The Eötvös number
260 (Eo), the ratio of buoyancy to surface tension, is defined as follows:

$$Eo = \frac{\left(\rho_l - \rho_g\right) g \, {d_B}^2}{\sigma} \quad \text{(Eq. 13)}$$

261 where d_B is the bubble diameter (m) and σ is the liquid surface tension (N/m).
262
263 To analyze the impact of the effects of contamination on hydrodynamics, two drag laws depending
264 on the Eötvös number were selected. On one hand, the drag law proposed by Dijkhuizen et al.
265 (2010), developed using direct numerical simulation (DNS) and without contamination effects, is
266 considered as representative of a perfectly clean bubble surface (Eq. 14).

$$C_{D0} = \frac{8}{3} \frac{Eo}{\frac{19}{3} + \frac{2}{3} Eo} \quad \text{(Eq. 14)}$$

267 On the other hand, the drag law proposed by Tomiyama et al. (1998), based on experimental results,
268 is considered as representative of classical experimental conditions with a slightly contaminated
269 system (Eq. 15).

$$C_D = max\left\{min\left\{\frac{24}{Re}(1 + 0.15Re^{0.687}), \frac{72}{Re}\right\}, \frac{8}{3}\frac{Eo}{(4 + Eo)}\right\} \quad \text{(Eq. 15)}$$

270 These drag laws are based on single bubbles rising in liquid. For bubble swarms, a corrective factor,
271 depending on gas hold-up, can be taken into account to consider a hindered slipping gas velocity
272 (Eq.16; Wallis 1961):

$$C_D = C_{D0}\left(1 - \varepsilon_g\right)^{-2} \quad \text{(Eq. 16)}$$

273
274 2.2.2.5 Hydrostatic pressure equation and impact on gas superficial velocity and bubble diameter

Hydrostatic pressure at a height z in a deep bubble column is given by Eq. 17.

$$P(z) = P_0 + \rho_m \, g \, (H - z) \quad \text{(Eq. 17)}$$

where P_0 is the atmospheric pressure (Pa), g the gravity constant (m/s²), H the column height (m), and ρ_m the mix density (or apparent density), defined as:

$$\rho_m = \rho_l \left(1 - \varepsilon_g\right) + \rho_g \varepsilon_g \quad \text{(Eq. 18)}$$

Where ρ_l and ρ_g are the liquid and gas densities, respectively (kg/m³).

Moreover, bubble diameter evolves with pressure according to the following equation (Pöpel and Wagner 1994; Fayolle et al. 2010), derived from the ideal gas equation when the mass transfer can be ignored in the mass balance (Eq. 19):

$$d_B = d_{B0} \sqrt[3]{\frac{P_0}{P}} \quad \text{(Eq. 19)}$$

where d_{B0} is the bubble diameter at atmospheric pressure P_0 (m), and d_B the bubble diameter at pressure P(z). The bubble diameter at atmospheric pressure is an input datum that must be measured or estimated since it depends on the gas sparger and water properties.

Gas superficial velocity j_{g0} at atmospheric pressure P_0 and superficial gas velocity j_g at pressure P(z) are bound through the following equation, which is also derived from the ideal gas equation:

$$j_g(z) = j_{g0} * \frac{P_0}{P(z)} \quad \text{(Eq. 20)}$$

2.2.3. Mass transfer calculation

Even though the hydrodynamic phenomena can be considered to reach a steady state, mass transfer is fundamentally a transient phenomenon, using as input the hydrodynamic variables previously calculated (gas hold-up, gas velocity, pressure, and bubble diameter along the column height). To

simulate oxygenation dynamics measured via reaeration tests (see 3.2), species transport equations are presented for oxygen in a two-phase flow as in Talvy et al. (2007a) and further modified in order to integrate the pressure effect for deep bubble columns.

When considering a perfectly mixed liquid without a liquid flow rate (batch bubble column), the oxygen concentration equation in the liquid is written as follows for a 1-D system:

$$\frac{\partial C_l(t)}{\partial t} = < \frac{k_L a(z)}{1-\varepsilon_g(z)} \left(C_l^*(z,t) - C_l(t)\right) > \quad \text{(Eq. 21)}$$

$$C_l^*(z,t) = He_{O2}(T)\, M(O_2)\, x_g(z,t)\, P(z) \quad \text{(Eq. 22)}$$

The oxygen concentration in the liquid (C_l) is expressed as a mass concentration and C_l^* is the saturation concentration at equilibrium. The variation of oxygen concentration in the liquid phase over time results from a transfer term from the gas to the liquid. The parameters k_La and ε_g are the mass transfer coefficient and gas hold-up, respectively, $He_{O2}(T)$ the Henry law coefficient at temperature T for oxygen solubility in water (1.24×10^{-5} mol/m^3/Pa at 25°C), $M(O_2)$ the oxygen molar mass (32 g/mol), $x_g(z)$ the local oxygen molar fraction in the gas phase at height z and P(z) the local hydrostatic pressure.

Because of the perfectly mixed liquid assumption, only one equation for the whole liquid volume is considered, and the parameters k_La, ε_g and C_l are taken as their average value in the column for the calculation. The oxygen concentration in the gas phase $C_g(z)$ can be calculated by the ideal gas equation from the oxygen molar fraction $x_g(z)$. As for the liquid, the oxygen concentration in the gas phase changes over time, although it is difficult to measure.

Thus, for low soluble gases, the 1-D transfer equation in the gas phase gives (Talvy et al., 2007):

$$\frac{\partial \varepsilon_g C_g(z,t)}{\partial t} + \nabla\, \varepsilon_g(z) C_g(z,t) U_g(z) = -k_L a(z)(C_l^*(z,t) - C_l(t)) \quad \text{(Eq. 23)}$$

The first term on the left side corresponds to the evolution over time and the height of the oxygen concentration in the gas phase, the second to the transport term of oxygen by the gas velocity and

315 the term on the right side is the oxygen transfer term from the gas to the liquid. In the gas phase,
316 neither diffusion nor reaction is considered, since the model applies for homogeneously dispersed
317 bubbly flow where no coalescence between bubbles occurs.
318 When solving the equation of the oxygen molar fraction in the gas phase, it gives an expression with
319 a first order discretization for the gas phase convective transport:

$$\frac{\partial x_g(z,t)}{\partial t} = -\frac{k_L a(z)}{\varepsilon_g(z) * \frac{M(O_2)}{RT}\left(P(z) - P_{vap}\right)}\left(C_l^*(z,t) - C_l(t)\right) - \frac{U_g(z)}{\Delta z}\Delta C_g(z,t) \qquad \text{(Eq. 24)}$$

320 where $k_La(z)$ is the local mass transfer coefficient, R the ideal gas constant (8.314 J/mol/K), and $U_g(z)$
321 the local bubble velocity. The gas concentration variation over time therefore results from a negative
322 transfer term from the gas to the liquid, and from a transport term related to the gas phase velocity.
323 Equation 24 is solved for each z-position in the column following the z-axis: the oxygen molar fraction
324 in the gas $x_g(z)$ is then calculated for each height over time with the local hydrodynamic parameters
325 solved from the equations provided in section 2.2.2. In this model, the hydrodynamic parameters
326 have a local impact on local mass transfer, but the reverse is not considered given that the oxygen
327 depletion in the gas phase can be ignored for the gas flow rate (Talvy et al. 2007a, Baeten et al.
328 2020).
329
330 2.2.4. Models for mass transfer coefficients
331 The mass transfer coefficient k_La could be expressed in terms of the interfacial area a and the liquid-
332 side mass transfer velocity k_L (m/s). To estimate the latter, there are several existing models and, as
333 for the drag coefficient, they depend on whether or not the bubble interface is contaminated (Dani
334 et al. 2007, Xu et al. 2018).
335 On one hand, the Higbie model is very commonly used and corresponds to the ideal case of perfectly
336 clean (non-contaminated) bubbles, which have a renewable interface: the diffusional oxygen transfer
337 in the liquid film surrounding gas bubbles occurs when the liquid elements reach the gas-liquid

interface and during a short contact time (t_C) they attain the concentration equilibrium with the interface. Under these conditions, the mass transfer coefficient is written as (Higbie 1935):

$$k_L = 2\sqrt{\frac{D}{\pi\, t_c}} = 2\sqrt{\frac{D\, G}{\pi\, d_B}} \quad \text{(Eq. 25)}$$

where k_L is the liquid side mass transfer coefficient (m/s), D the diffusion coefficient of oxygen in water (m^2/s), t_c the contact time (s), G the gas slip velocity (m/s) and d_B the bubble diameter (m).

On the other hand, the case of completely contaminated bubbles is described by the Frössling model, which assumes that bubbles have a rigid, non-renewable interface. The mass transfer coefficient is then expressed as (Frössling 1938):

$$k_L = \frac{D}{d_B} * (2 + 0.6 * Re^{0.5} * Sc^{0.33}) \quad \text{(Eq. 26)}$$

where the Reynolds and Schmidt dimensionless numbers are defined as:

$$Re = \frac{\rho_l\, d_B\, G}{\mu_l} \quad \text{(Eq. 27)}$$

$$Sc = \frac{\mu_l}{\rho_l\, D} \quad \text{(Eq. 28)}$$

where ρ_l and μ_l are respectively density (kg/m^3) and the dynamic viscosity (Pa.s) of the liquid.

In practice, the k_L coefficients calculated with the Frössling correlation are much lower than with the Higbie model, i.e., that bubbles are contaminated and thus mass transfer is hindered due to the impurity molecules (e.g., surfactants) adsorbed at the bubble surface. The k_L coefficients measured are thus always between these two asymptotic and ideal cases (Xu et al. 2018).

2.2.5 Volumetric bubble interfacial area a

The interfacial area of spherical bubbles is given by (Eq. 29):

$$a = \frac{6}{d_B}\varepsilon_g \quad \text{(Eq. 29)}$$

where a is the bubble's interfacial area (m^2/m^3), d_B the bubble's diameter (m), and ε_g the gas hold-up (-).

If the bubbles are ellipsoidal, a correction factor that includes bubble eccentricity K (the ratio of major axis to minor axis) is taken into account (Cockx et al. 1997, Colombet et al. 2011):

$$a = \frac{6}{d_B}\,\varepsilon_g\, f(K) \qquad \text{(Eq. 30)}$$

$$f(K) = \frac{1}{2\,K^{1/3}} * \left(K + \frac{\ln(K + \sqrt{K^2 - 1}}{\sqrt{K^2 - 1}}\right) \qquad \text{(Eq. 31)}$$

Ellipsoidal bubbles have a higher interfacial area than spherical ones, thus f(K) is always higher than 1.

2.2.6 Numerical method, boundary and initial conditions.

First, the 1D steady state model runs using Matlab® for a fully developed bubbly flow (equations 5 to 20 with the algebraic solver function fsolve) in order to obtain axial profiles of the gas fraction, the gas velocity, the pressure and the bubble diameter along the column height (50 layers along z) as a function of the input parameters (inlet bubble diameter, gas flow rate, column height). Then, mass transfer between the gas and the liquid phase are calculated from hydrodynamics results with a transient solver (ode23t function for equations 21 to 24 with closure relations 25 to 31). This one-way coupling hydrodynamics and mass transfer is only valid with the assumptions that the mass transfer does not modify hydrodynamic parameters (i.e. similar molar flow rates in the gas phase).

For all the simulations presented hereafter, the initial molar fraction of oxygen in the gas was set to the inlet atmospheric condition at the bottom of the column (xg(z) = 0.21) for all discretization layers along column height, physically corresponding to the fact that fresh air is continuously supplied in the column from the bottom, so that the oxygen molar concentration in the gas at the inlet does not vary. The initial dissolved concentration in the liquid phase was considered as an initial condition: depending on the simulated experiments, its value was set to the initial experimental dissolved oxygen concentration (mostly equal to zero). Finally, the simulated length of time is also adjustable,

and it has to be long enough to allow the system to reach an equilibrium state, i.e. when the oxygen concentration in liquid is equal to the saturation value. The time to reach steady state conditions depends on the mass transfer from bubbles and on experimental conditions. For the bubble columns considered, the simulated time period lies between 500 and 20,000 s.

3. Results and discussion

3.1 Hydrodynamic characterization of the datasets studied

A pragmatic approach is applied to select the combinations of correlations and closure laws that make it possible to obtain a reliable description of the three experimental datasets with the 1-D model, in terms of global gas hold-up changes with the superficial gas velocity. The combinations of the closure laws considered are presented in Table 3.

Table 3. Selected combinations of closure laws for appropriated modelling of each datasets.

Dataset	Pressure effects on bubble size and gas superficial velocity	Contamination effects regarding hydrodynamics (via the drag law considered)	Collective effects (via Eq. 16)
D1	Included	Contaminated (Tomiyama drag law)	Included
D2	Included	Contaminated (Tomiyama drag law)	Included
D3	Included	No contamination (Dijkhuizen drag law)	Included

The selected model structures include pressure and collective effects for all datasets. The drag law correlation of Tomiyama et al. (1998) is used for the datasets obtained with unfiltered tap water (D1 and D2), whereas the correlation proposed by Dijkhuizen et al. (2010) is used to simulate the hydrodynamics for the dataset obtained with filtered tap water (D3). For each dataset, the model including the closure laws presented in Table 3 is called the “base model” in the following.

Figure 3 presents the simulated and experimental gas hold-up as a function of the superficial gas velocity.

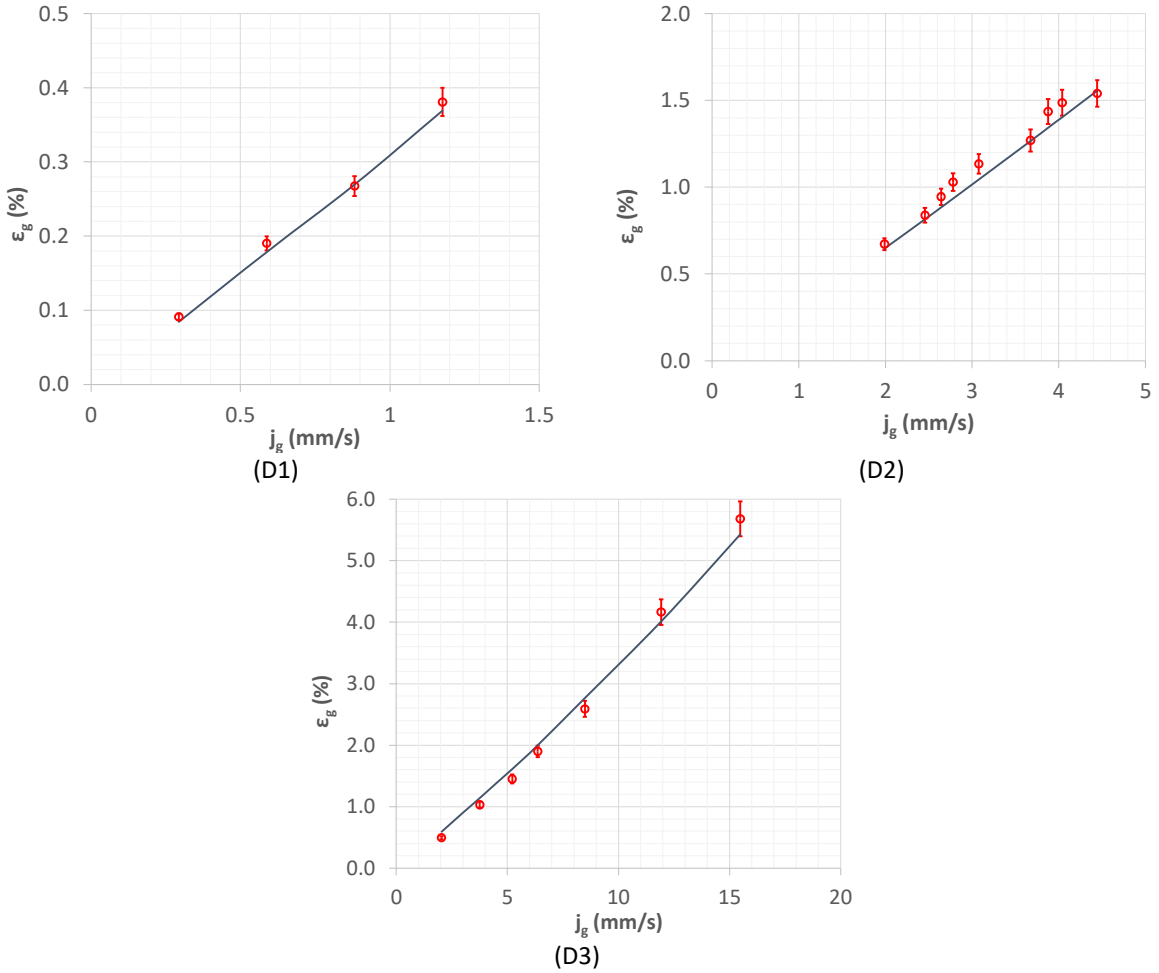

Figure 3. Global gas hold-up for different superficial gas velocities and for each dataset – Base models (**O**: Experimental data / ——: Base model / Error bars: ± 5%)

Good accuracy is obtained comparing simulated and experimental values (with an average difference between the experimental and simulated values of 4.6, 5.1 and 8.0 % for D1, D2 and D3 respectively). These results highlight that the 1-D model, considering appropriate closure laws, is relevant to model steady-state hydrodynamics of the bubble column along the vertical direction. The model is used in the following section in order to analyze the impact of selected closure laws and physics and to propose a deeper analysis of the different datasets on the basis of the effects considered (pressure, contamination effects and collective effects). The impact of the effects considered is analyzed per dataset by modifying the associated closure law in the model presented in Table 3.

3.1.1. Analysis of the pressure impact on hydrodynamics

The pressure effects on hydrodynamics is integrated into the model via bubble diameter (Eq. 19) and gas superficial velocity (Eq. 20), in order to take into account gas volume expansion (and associated bubble size) with variation in the local hydrostatic pressure. Since the mean bubble diameter varies with pressure following a cubic root law, the impact of pressure on this parameter is not as high as for gas superficial velocity.

Figure 4 presents the changes in the overall hold-up as a function of the superficial gas velocity for the modified model (i.e. without considering the pressure effect on bubble size and superficial gas velocity along z), the base model (Table 3) and the experimental data for each dataset.

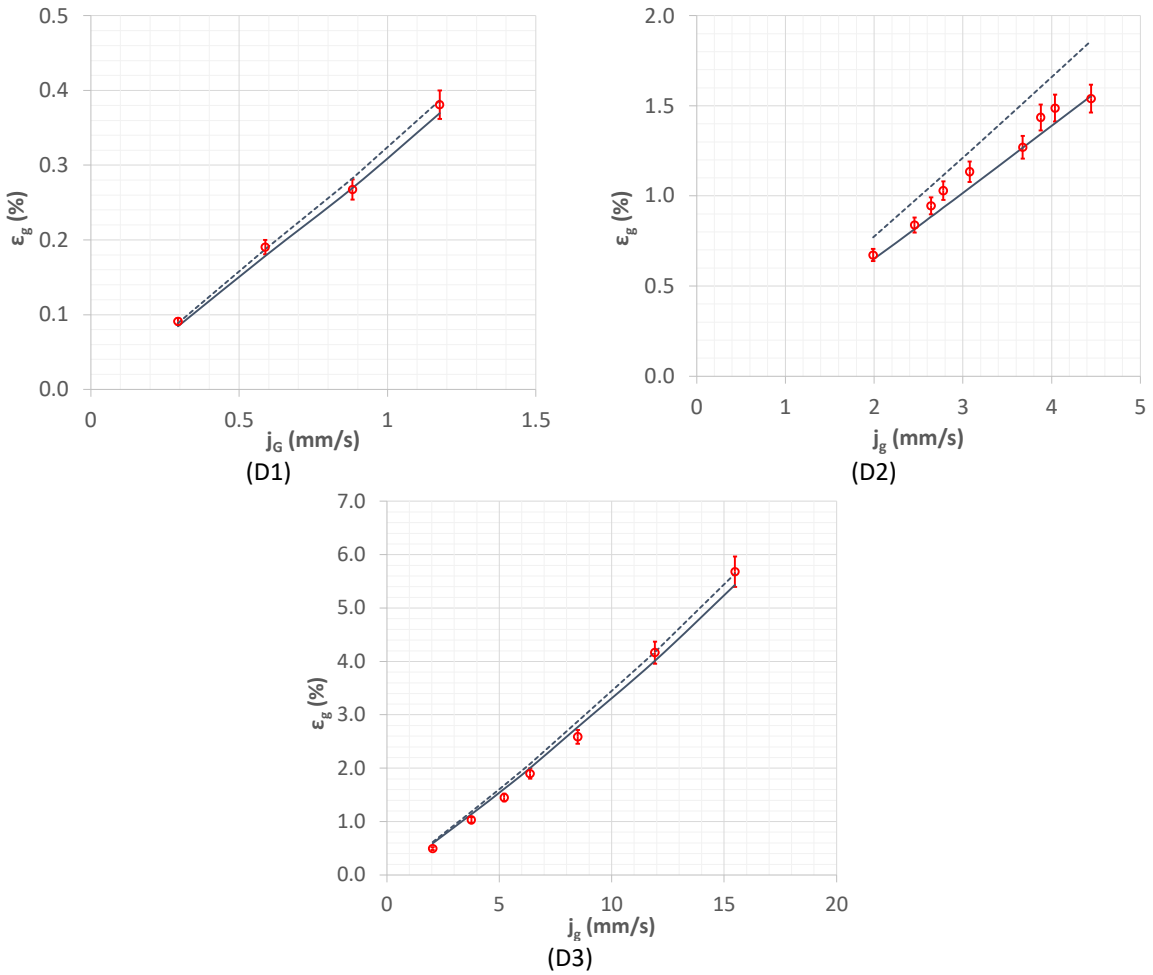

Figure 4. Overall gas hold-up for different superficial gas velocities and for each dataset. Impact of the pressure effects (**O**: Experimental data / ▬: Base model (with pressure effects) / ▪▪▪▪ :Modified model (without pressure effects) / Error bars: ± 5%)

As expected, the deviation due to the pressure effects is the most significant for dataset D2, because the water height is highest (4.5 m). The simulated gas hold-up is lower when the pressure effects are considered (28 % of the overall gas hold-up overestimation when the pressure impact is not accounted for), and experimental points are better described in that case. For datasets D1 and D3, since the water height is low (1.3 and 0.8 m, respectively), the simulation results are less affected.

For deep bubble columns, the impact of hydrostatic pressure on the gas-liquid hydrodynamics (i.e. ε_g) along the column height are significant mainly due to its influence on gas superficial velocity (and to a lesser extent due to its influence on bubble size) and must be taken into account to appropriately model gas hold-up. For low soluble gases and a bubble size between 3 and 5 mm, the slip velocity is almost constant and the effect of local pressure on gas hold-up can be estimated considering a linear correlation, deduced from the ideal gas law:

$$\frac{\varepsilon_g}{\varepsilon_{g0}} = \frac{1}{2}\left(1 + \frac{P}{P_0}\right) \approx 1 - \frac{\rho_m g H}{2P_0} \approx 1 - \frac{H}{20} \qquad \text{(Eq. 32)}$$

Using Eq. 32, the reduction of the overall gas hold-up over the column height can be roughly estimated at 5% per meter (1/20).

3.1.2. Analysis of contamination effects on hydrodynamics

The impact of contamination effects is then analyzed via the drag law considered included in the model.

Since the bubbles are ellipsoidal, drag laws applied to the three datasets are focused on correlations depending on the Eötvös number (see Table 3). Since different water qualities could be considered in regards to experimental conditions (clean water [filtered water] for D3 and contaminated water [tap water] for D1 and D2), consistent drag correlations were selected to analyze their impact on hydrodynamics. As indicated in section 2.2.2.4, Dijkhuizen's drag correlation was selected for clean bubble surfaces, whereas Tomiyama's was considered for contaminated bubbles. Please note that the base model for D3 included Dijkuizen's drag law, whereas the base model for D1 and D2 included Tomiyama's drag law.

Figure 5 presents the overall hold-up as a function of the superficial gas velocity for models including Dijkhuizen's or Tomiyama's drag correlations and the experimental data for each dataset. The other closured laws considered in the respective models remain similar to Table 3.

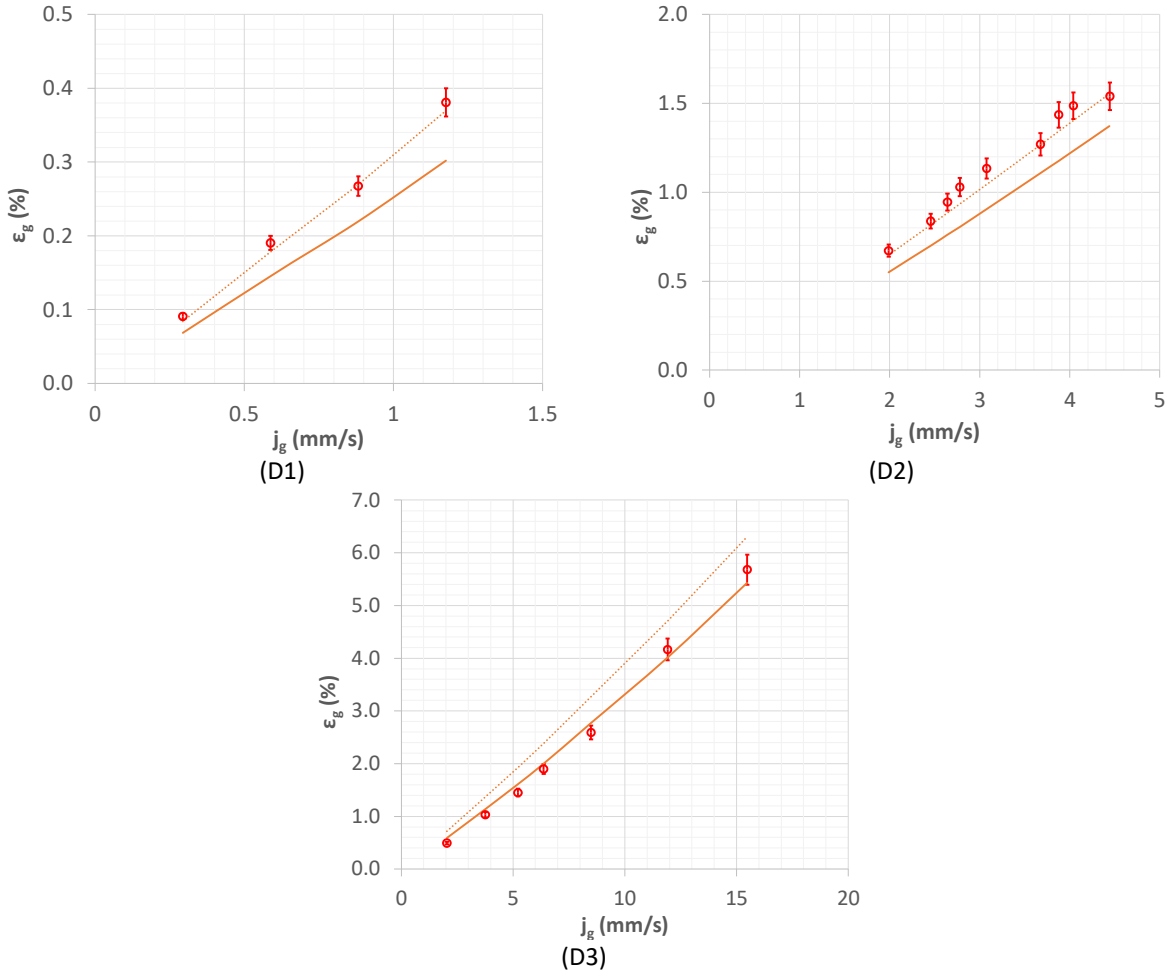

Figure 5. Overall gas hold-up for different superficial gas velocities and for each dataset (**O**: Experimental data / ▬: Dijkhuizen's drag correlation / ▪▪▪▪ : Tomiyama's drag correlation / Error bars: ± 5%)

The gas hold-up modeled was significantly impacted by the modification of the drag law considered, related to the contamination effects. The mean modeled values considering Tomiyama's drag correlation are from 15 to 22 % higher in comparison with modelled results obtained with Dijkhuizen's drag law, depending on the dataset considered and on the gas flow rate. The results obtained with the model that included Dijkhuizen's drag law fit the experimental points of dataset D3 better. This is a reasonable result related to the water quality of this dataset, which could be considered close to clear water (filtered water) and to the air diffuser (capillaries): the high air flow rate applied induces a lower contact time between nascent bubbles and liquid during bubble

455 formation along the capillary (Loubière et al. 2003). In the case of datasets D1 and D2, the
456 experimental data are better described by the model integrating Tomiyama's drag correlation. This is
457 in accordance with the water quality during these experiments (tap water). Considering
458 hydrodynamics, the bubble surface for datasets D1 and D2 must be considered as contaminated,
459 whereas it must be considered as clean for dataset D3. These results highlight that drag laws must be
460 selected in accordance with actual operating conditions in order to consider bubble interface
461 contamination by real water.
462 Due to the narrow gas hold-up range in the datasets selected, the deviation in the simulation
463 hydrodynamics results related to the collective effects are less significant than for the effects
464 discussed above. The mean deviation is lower than 5%, with the highest values observed for dataset
465 D3 due to the wider range studied in terms of gas hold-up. From the model (using Eq. 16), we can
466 estimate, by limited development of Eq. 12, that the gas fraction increase is around 2% of relative
467 deviation per percentage of gas hold-up. Therefore, the collective effect cannot be ignored for gas
468 hold-up from 3% (deviation greater than 6%, the data are given in supplementary material – Figure
469 S1).
470
471 3.2 Mass transfer results
472 The simulated time variation of the dissolved oxygen concentration in liquid $C_l(t)$ allows one to
473 calculate an overall K_La coefficient for the entire bubble column (Cockx et al. 2001) through the
474 following classical equation:

$$C_l(t) = C_l^* - (C_l^* - C_{l0})\, e^{-K_L a * t} \qquad \text{(Eq. 33)}$$

475 where C_{l0} is the dissolved oxygen concentration at t=0 (mg/L) and K_La is the overall mass transfer
476 coefficient (h^{-1}). For example, the experimental dissolved oxygen over time obtained by Duran et al.
477 (2016) was compared with simulated dissolved oxygen (cf. supplementary materials – Figure S2).
478 K_La is also called the apparent mass transfer coefficient, since it assumes a constant equilibrium
479 oxygen concentration C_l^*, although it actually varies with the oxygen concentration in gas during

480 reoxygenation (see Eq.22). Furthermore, the K_La coefficient is considered as a whole, with no
481 distinction between K_L and a. This overall apparent K_La coefficient differs from the local k_La
482 coefficient, which results from the multiplication of the local liquid-side mass transfer coefficient k_L
483 (for example modeled with the Higbie penetration model) and the local interfacial area a. This local
484 k_La coefficient varies locally essentially with z in a bubble column and can be averaged in the whole
485 liquid volume. Moreover, it is quite difficult to determine experimentally k_L and a separately in a real
486 bubble column (Colombet et al. 2011, 2015).
487 In the following section, global K_La values determined experimentally are compared with simulated
488 global K_La coefficients with the Higbie and Frössling models for k_L, in order to see which transfer
489 model fits the experimental points better when contamination of the bubbles is not fully controlled
490 (real water).
491
492 3.2.1 Comparison of the Higbie and Frössling transfer models
493 Figure 6 presents the overall K_La versus the superficial gas velocity for the three experimental
494 datasets and associated modelling results.

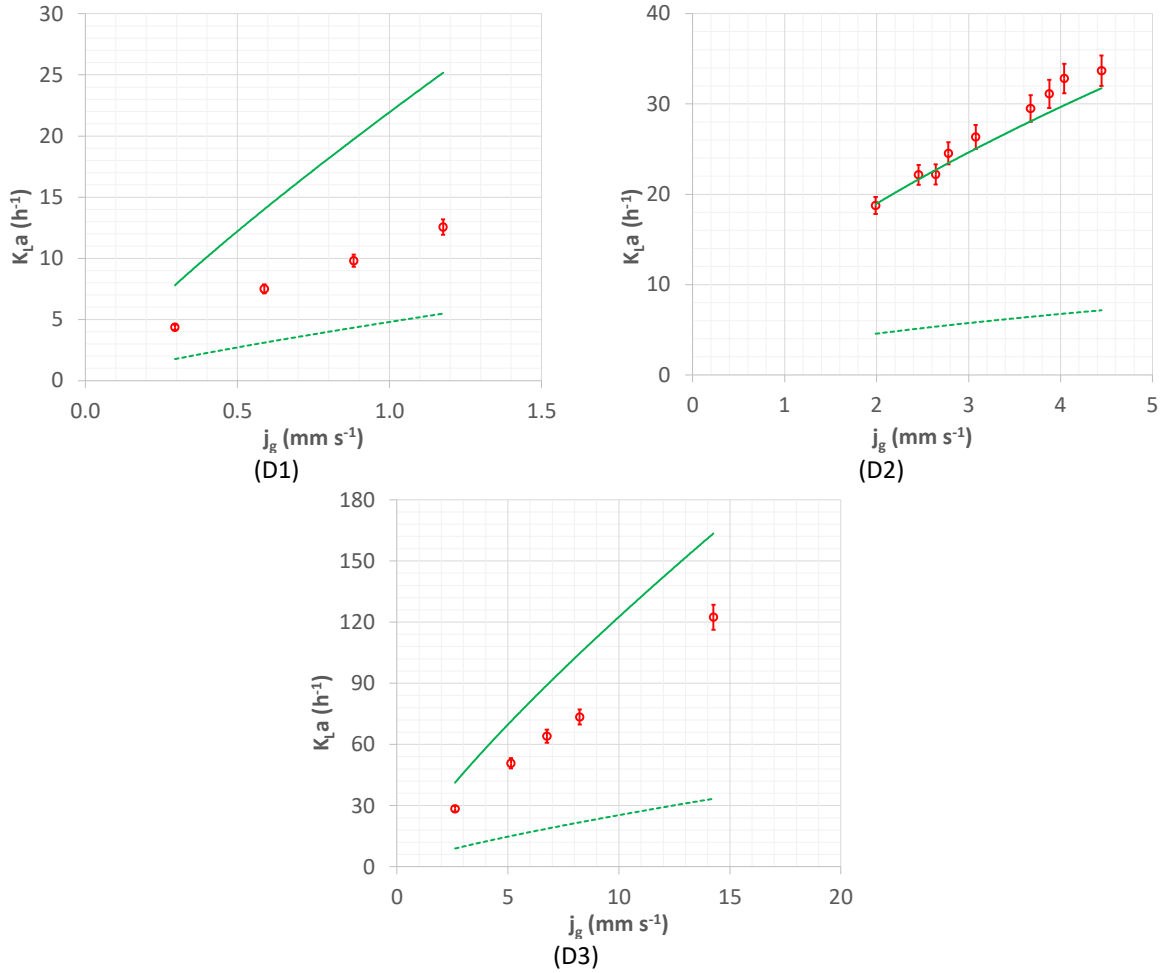

Figure 6. Overall K_La transfer coefficients for different superficial gas velocities and for datasets D1–D3 (**O**: Experimental data /▬: Modelled global K_La with Higbie model / ▬ ▬: Modelled global K_La with the Frössling model / Error bars: ±5%)

495

496 For dataset D3, the mass transfer is closer to the Higbie model (clean bubble surface) than to the
497 Frössling model (contaminated bubble surface). From the 1-D transient simulation, it can be deduced
498 that the transfer interface is slightly contaminated (bubble size between 2.3 and 3.4 mm) even if the
499 hydrodynamic simulation results show that filtered water does not reduce the bubble velocity
500 (apparent clean interface for the drag force).

501 For dataset D2, the water quality is lower (tap water) and consequently induces contamination of the
502 bubble surface, affecting the drag coefficient, which is confirmed by the hydrodynamics results (see
503 section 3.1.2). However, Figure 6 highlights that the overall mass transfer is not really impacted
504 because the transfer simulation shows that the non-contaminated Higbie model (clean bubbles)

505 works better than the Frössling model (fully contaminated bubbles). This apparent contradiction can
506 be explained by the fact that for dataset D2, the bubbles are larger and ellipsoidal, between 3 and 4
507 mm. In this case, the contaminants at the bubble interface are transported to the rear of the bubble
508 where local mass transfer is drastically lower than at the front where interface renewal is greater
509 (Dani et al. 2007, Figueroa and Legendre 2010). For this reason, the bubble slip velocity could be
510 reduced for large bubbles in tap water as observed in Figure 5, but not the mass transfer velocity
511 (Figure 6).
512 For dataset D1, experimental K_La values are much lower compared to D2 and D3 and seem slightly
513 closer to the Frössling model. This can be related to the fact that bubbles in these experiments are
514 significantly smaller and spherical (below 1.8 mm) and more likely to be contaminated, with a more
515 rigid and less renewable bubble interface. In this case, the slip velocity behaves like a completely
516 contaminated bubble and the mass transfer velocity is clearly lower than for larger bubbles also with
517 tap water (as observed for dataset D2).
518 These results confirm that when tap water is used, the Higbie transfer model is the most accurate for
519 large bubbles (dataset D2, bubble size, 3.0–4.0 mm) and less relevant for small ones (dataset D1,
520 bubble size, 1.5–1.8 mm), with significant contamination effects. For filtered water, the Higbie model
521 is also the most suitable, although the presence of small contaminants could have slightly reduced
522 the mass transfer velocity for intermediate bubble size (2.3–3.4 mm) because the water could not be
523 considered as really pure (Colombet et al. 2015) except when rigorous experimental conditions are
524 maintained with ultra-pure water. A complementary discussion on transfer contamination is detailed
525 in section 3.2.3 after analysis of the depletion effect which can imply bias in transfer velocity
526 estimation.
527
528 3.2.2 Comparison of mean local k_La and overall K_La: the oxygen depletion effect
529 In the previous discussion, the apparent K_La is compared to the simulation results with two
530 asymptotic models for clean bubble interfaces (Higbie model) and fully contaminated ones (Frössling

model). During this comparison, the pressure effect on the gas fraction, the bubble diameter and the oxygen saturation was modeled to take into account all the relevant physical phenomena that modify hydrodynamic and mass transfer parameters. With the "base model" (Table 3), it is also possible to clarify the effect of pressure and height on the mass transfer. In Figure 8, experimental overall K_La values are compared to both simulated overall K_La coefficients and to mean local values (spatial average $<k_La>$) calculated using the Higbie transfer model for simplicity.

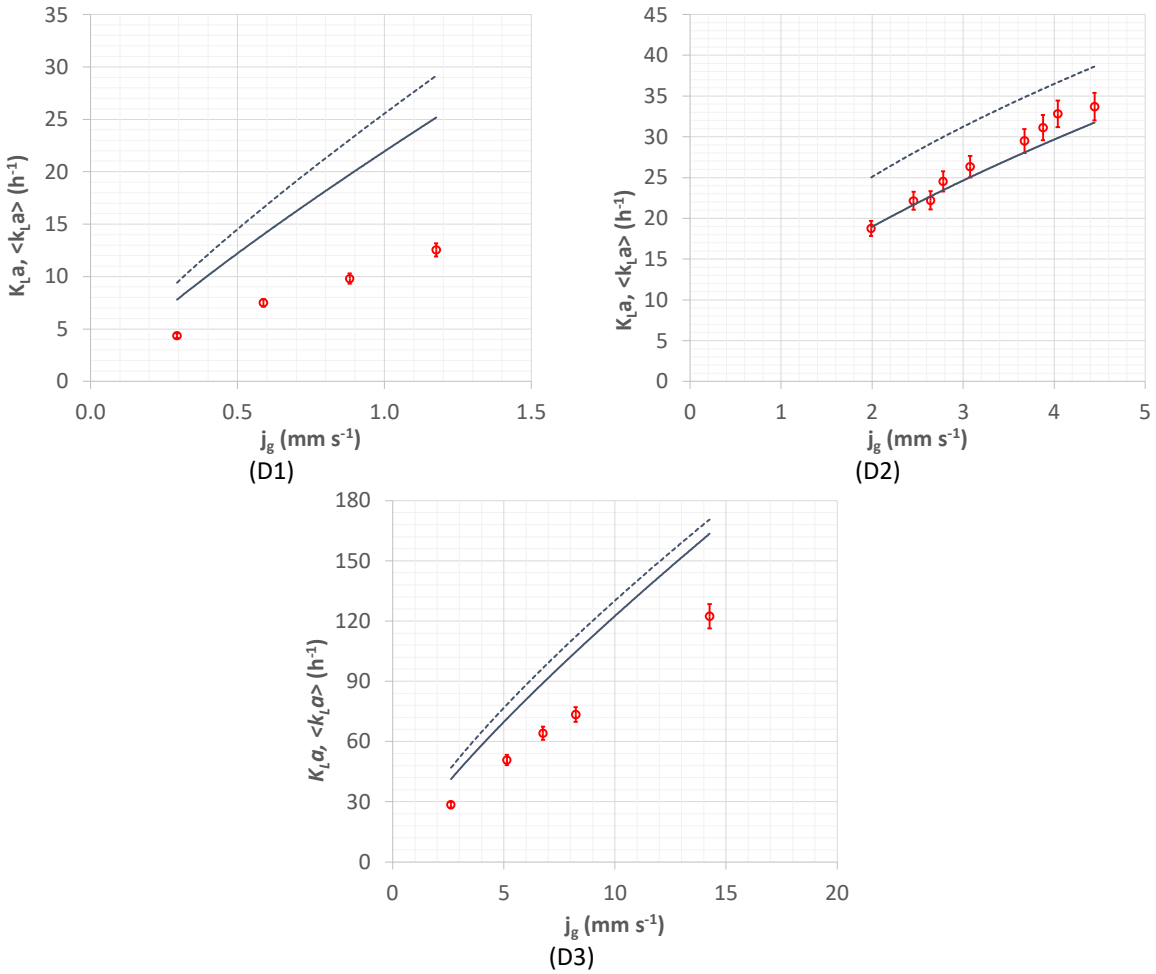

Figure 7. Experimental and modeled overall K_La and mean local $<k_La>$ for different superficial gas velocities and for datasets D1–D3 (**O** : Experimental global K_La /▬ : Simulated global K_La with the Higbie model /▪▪▪ : Simulated spatial average $<k_La>$ with the Higbie model / Error bars: ±5%)

The simulated global K_La coefficients are systematically lower than the simulated mean local $<k_La>$ coefficients, the difference stemming from the oxygen depletion in the gas (due to the column height) and thus a decrease of the equilibrium concentration C_l^* (Eq.24). Simulated global K_La

coefficients describe the experimental points more accurately since this parameter is deduced from reoxygenation curves versus time as for the experimental data, especially for dataset D2. Indeed, oxygen depletion in the gas is significant due to the high column height (4.5 m of water). For the other datasets, given the high superficial gas velocity and the low column height in the case of D3 (0.76 m), the difference between mean local and global K_La is the least significant. Surprisingly for dataset D1, since the column height is relatively low (1.3 m) and the superficial gas velocity is very low, the difference between the two K_La coefficients modeled is also relatively substantial (mean difference, 55%)

To understand and model this depletion effect in the gas, a simplified analysis is proposed in the following section.

3.2.3. When mean local $\langle k_La \rangle$ differs from overall K_La: modeling the depletion effect

The following development aims at explaining more deeply the effect of superficial gas velocity, column height and other process parameters on oxygen depletion. Compared to the mass transfer time ($1/K_La$), the bubble convection time or residence times (H/U_g) are smaller. The convection time and mass transfer time values are provided in the supplementary materials for the three datasets (Table S1).

Moreover, oxygen depletion in the gas occurs essentially at the beginning of the reoxygenation process, during a transient period ($t << 1/K_La$) when the oxygen concentration in the liquid $C_l(t)$ is close to 0 mg/L. During this transient period, Eq. 23 becomes:

$$\nabla\, \varepsilon_g C_g(z) U_g = -k_L a (C_l^*(z) - 0) \qquad \text{(Eq. 34)}$$

It appears that the depletion in the gas is given by the mass transferred. By estimating the oxygen saturation with the Henry' law (Eq. 22) and the interfacial area (Eq. 29), with the exchange coefficient m (Talvy, 2007), Eq. 34 becomes:

$$\nabla\, \varepsilon_g C_g(z) U_g = -k_L \frac{6.\ \varepsilon_g}{d_B}.m.C_g(z) \qquad \text{(Eq. 35)}$$

564 with $m = He_{O2}.RT$.

565 Assuming that the gas velocity is kept constant along the height of the bubble column, the
566 integration gives the following variation in the concentration along z:

$$\varepsilon_g C_g(z) = \varepsilon_{g0} C_{g0}. e^{-k_L \frac{6}{d_B}.m.\frac{z}{U_g}} \quad \text{(Eq. 36)}$$

567 The depletion in the gas (C_g/C_{g0}) decreases exponentially with (i) the mass transfer velocity k_L, (ii) the
568 solubility m (iii) the distance from the diffuser z, and (iv) the inverse of bubble size and the associated
569 slip velocity.

570 In this equation, $\varepsilon_g C_g$ is the mass of soluble gas per unit of volume (m_g) by introducing a depletion
571 factor (DF) for the whole column as:

$$DF = k_L \frac{6}{d_B}.m.\frac{H}{U_g} \quad \text{(Eq. 38)}$$

572 It is possible to estimate the decreasing ratio of mass in the gas along the height the bubble column
573 using Eq. 39:

$$\frac{\mathrm{m}_g}{\mathrm{m}_{g0}} = \frac{\varepsilon_g C_g}{\varepsilon_{g0} C_{g0}} = e^{-DF.\frac{z}{H}} \quad \text{(Eq. 39)}$$

574

575 For example, the depletion factor for D1 and D2 are close to 0.3 and 0.4, respectively, which
576 corresponds to depletion loss in the gas of 26% and 33 % using Eq. 38 at the top of the bubble
577 column. For dataset D3, the depletion factor is close to 0.05 and the decrease in the oxygen molar
578 fraction in the gas is lower than 5%. In our study, as the solubility is constant and the mass transfer
579 velocity k_L is quite constant for millimetric bubbles for oxygen, the substantial variation in the
580 depletion factor is mainly related to the length ratio H/d_b, which is about 800, 1200 and 200 for
581 datasets D1,D2 and D3, respectively. To illustrate the accuracy of the depletion model (Eq. 39), Figure
582 10 presents the oxygen molar fraction in the gas as a function of the distance from the diffusers at
583 the initial time (t=0) and in the stationary state (t>>1/ $K_L a$) for D1 and D2 when the depletion effect is
584 significant (Figure 7).

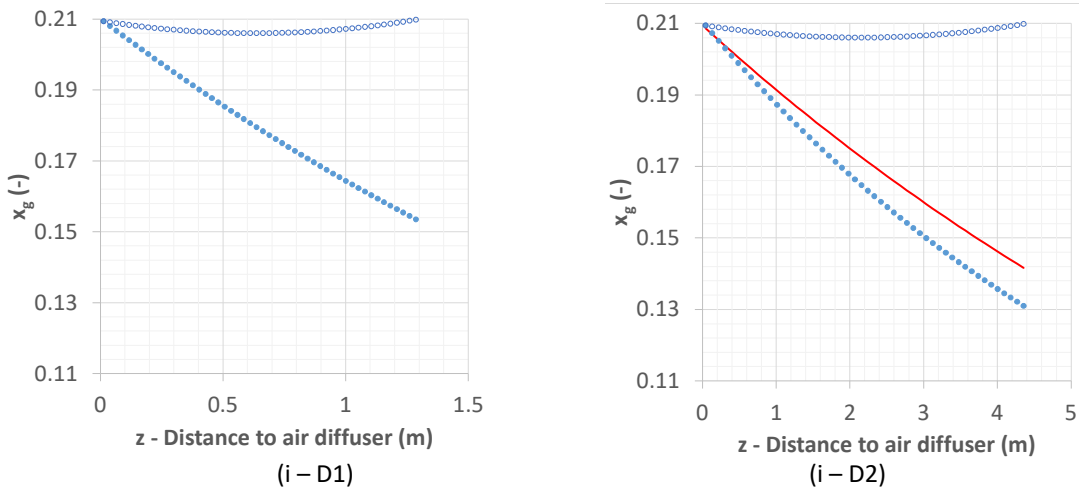

585 **Figure 10.** x_g as a function of z (distance from the diffuser) – Modelled for C_l = 0 mg/L (●) / Depletion law for C_l

586 = 0 mg/L (——)/ Modelled (○) for Cl = Cl* - j_g = 1.2 and 4.4 mm/s for D1 and D2 respectively

587

588 The oxygen depletion estimated with the relation (Eq. 39) is in good accordance with the

589 comprehensive 1D model. The depletion factor (Eq. 38) can then be used to identify the

590 experimental conditions inducing a significant impact of the gas depletion effects on the global mass

591 transfer coefficient K_La.

592 This depletion effect is clearly increased by (i) a long bubble residence time (H/U_g=4.3 s and 18.3 s for

593 D1 and D2, respectively), (ii) the high solubility of the gas considered passing into the liquid phase

594 (here m = 0.0034 is relatively low for oxygen in water) and (iii) the low transfer time at the bubble

595 scale (d_B/k_L=2.8 s and 9.4 s for D1 and D2, respectively).

596 In comparison with the relative simplicity of the estimation of the mean bubble residence time (H/U_g)

597 in a bubble column, it is much more difficult to determine the bubble transfer time (d_B/k_L) precisely,

598 which can vary along the column height due to substantial bubble size changes with increasing

599 hydrostatic pressure. However, this bubble transfer time could be estimated through the inverse

600 ratio of the global volumetric transfer coefficient to the global gas fraction (K_La/ε_g). This last

601 parameter is also close to the transfer number N_T (Figure 2) but both approximations imply a certain

602 bias because all the nonlinearity effects on average values are ignored.

603

3.2.4 Mass transfer and bubble contamination angle

In this section, the level of bubble contamination is studied through their contamination angle, according to the theory developed by Sadhal and Johnson (1983). The level of bubble contamination is characterized through a contamination angle, corresponding to the contaminated interface occupied by the adsorbed contaminants at the bubble surface, expressed as the angle between the rear of the bubble and the limit of the contaminated surface. The contamination angle varies between 0° and 180°, depending on whether the bubble surface is completely clean or completely contaminated, respectively. For all experimental data, the experimental global K_La coefficients lie between the ideal K_La coefficients obtained with the Higbie and Frössling mass transfer models (Figure 6). The contamination angle is obtained from the dimensionless drag coefficient with the following correlation (Sadhal and Johnson 1983; Dani 2007):

$$C_D^*(\theta_{cap}) = \frac{1}{2\pi}(2\theta_{cap} + \sin(\theta_{cap}) - \sin(2\theta_{cap}) - \frac{1}{3}\sin(3\theta_{cap})) \quad \text{(Eq. 38)}$$

with θ_{cap} the drag contamination stagnant cap angle (in radian).

On the other hand, the dimensionless drag coefficient $C_D^*(\theta_{cap})$ is related to the Sherwood numbers of the bubble (experimental), of a completely clean bubble (Higbie correlation) and of a completely contaminated bubble (Frössling correlation) as follows (Takemura and Yabe 1999, Dani 2007, Xu et al. 2018):

$$C_D^*(\theta_{cap}) = 1 - \left(1 - \frac{Sh - Sh_{Higbie}}{Sh_{Frössling} - Sh_{Higbie}}\right)^2 \quad \text{(Eq. 39)}$$

with Sh the experimental Sherwood number, Sh_{Higbie} the Sherwood number of a completely clean bubble and $Sh_{Frössling}$ the Sherwood number of a completely contaminated bubble.

The Sherwood number is defined as follows:

$$Sh = \frac{k_L * d_B}{D} \quad \text{(Eq. 40)}$$

624 with k_L the experimental mass transfer velocity estimated from the experimental reoxygenation
625 curves using the 1-D model (via iterative calculation).
626
627 Table 4 presents the Sherwood numbers of the real bubbles calculated from the comprehensive
628 model of a completely clean and a completely contaminated equivalent bubble. The transfer
629 contamination angle is then deduced from Eq. 38 for datasets D1 and D3.
630 **Table 4.** Sherwood numbers and contamination angle and for the experimental dataset D1 and D3

Dataset	j_g expressed at P_{atm} (mm/s)	d_b expressed at P_{atm} ($\times 10^{-3}$ m)	k_L ($\times 10^{-4}$ m/s)	Sh_{exp} (-)	Sh_{Higbie} (-)	$Sh_{Frössling}$ (-)	Θ_{cap} (°)
D1	0.29	1.48	3.80	313	625	120	105
	0.59	1.69	3.47	286	568	109	105
	0.88	1.71	3.01	248	562	108	113
	1.18	1.83	3.00	247	536	103	110
D3	2.62	2.34	3.85	450	699	134	88
	5.14	2.58	3.65	471	716	138	86
	6.76	2.72	3.58	487	723	140	84
	8.23	2.84	3.42	486	729	141	85
	14.26	3.28	3.47	569	749	147	73

631
632 For each dataset, the contamination angles vary slightly with superficial gas velocity and the water
633 quality appears to be specific for each dataset.
634 For dataset D1, the transfer contamination angle lies between 105 and 113°, which indicates a high
635 level of bubble contamination that substantially reduces the mass transfer compared to an
636 equivalent clean bubble (around 50%). This angle designation is consistent with the fact that the
637 experimental hydrodynamics (i.e. ε_g) of dataset D1 was adequately reproduced using a drag
638 coefficient set for contaminated bubbles (Figure 5).
639 For dataset D3, lower transfer contamination angle values were obtained in comparison with dataset
640 D1. Even if the water is very clean (filtered tap water), the mass transfer is still hindered compared to
641 a clean equivalent bubble (between 24 and 36%), but the decrease of the drag coefficient due to the
642 water contamination remains negligible (Figure 5).

For dataset D2**,** since experimental global K_La values fit well with the Higbie model (see Figure 6), it can be deduced that bubbles have transfer contamination angles close to zero and are equivalent to completely clean bubbles. This means that the greater the bubble size, the less the drag contamination impact has an effect on mass transfer:1.5-, 2.5- and 3.5-mm bubbles correspond to 105°, 88° and 0° contamination angles, respectively. This means that when the bubble size increases, it becomes ellipsoidal and the mass transfer occurs intensively at the front of the bubble where the transfer contamination tends to become negligible (Dani et al., 2021).

3.2.5 Discussion on mass transfer modeling

Hydrodynamic parameters calculated with the 1D model in steady state conditions (bubble diameters, gas hold-up and gas velocity) were validated and then used in order to calculate reoxygenation and global K_La mass transfer coefficients. A distinction was made between mean local $<k_La>$ and apparent global K_La. The latter is calculated from simulated curves of dissolved oxygen concentration over time, and takes into account oxygen depletion in the gas phase and therefore the variation in the equilibrium concentration versus time. A comparison with the experimental data of global K_La therefore provides accurate results, especially for deep bubble columns and/or a low gas flowrate when oxygen depletion in the gas increases (Eq. 36). The depletion factor (Eq. 37) is adapted to characterize and interpret situations where the effects of oxygen depletion influence the gas–liquid transfer due to gradient in the gas phase composition.

Moreover, for the three experimental datasets, the Higbie and Frössling mass transfer models were used to interpret mass transfer results with no bias related to the quality of the liquid phase composition (Baeten et al. 2020). When tap water was used for experiments (D1 and D2), the smaller the bubbles, the more they were contaminated. Consequently, the global mass transfer coefficient could be drastically reduced (up to 50% by model comparison with clean bubbles with dataset D1). Surprisingly, even if contamination reduces the slip velocity in dataset D2, mass transfer is not affected by the contamination because the bubbles are big enough to be ellipsoidal: in this case the

669 transfer occurs mainly at the front of the bubble interface (Dani et al. 2006). For dataset D3 obtained
670 using filtered water, the mean slip velocity of bubbles corresponds to that obtained for pure water.
671 However, for this relatively clean water, the bubble surface was still characterized as partially
672 contaminated (contamination angle estimated at 100°).
673 In the context of oxygen transfer in aeration processes, it is then possible to ignore the effect of
674 contamination with tap water for ellipsoidal bubbles greater than 3 mm (as for dataset D2).
675 However, for small bubble sizes (under 2 mm), the quality of the tap water can drastically reduce the
676 mass transfer (more than 50% compared to clean bubbles). In both situations, depletion effects are
677 substantial in deep bubble columns but must also be taken into account for relatively low column
678 height and specific studies (low mean bubble size or high solubility of the component studied).
679 In addition, the impact of eccentricity on the modeled mass transfer coefficient is given in
680 supplementary information (Figure S3). For datasets D2 and D3, the mean local $<k_La>$ values modeled
681 are slightly higher when eccentricity is taken into account. To remain physically consistent,
682 eccentricity must be systematically considered to calculate the interfacial area of ellipsoïdal bubbles.
683

684 **4. Conclusions**

685 The main conclusions of this study are:

686 • The proposed 1-D model is able to reproduce experimental hydrodynamic (global gas hold-
687 up) for three different experimental datasets in bubble columns with an air/clear water
688 system. The closure laws considered must be rigorously selected in order to integrate the
689 impact of contamination, collective and pressure effects on hydrodynamics, and the mass
690 transfer parameters. Depending on the experimental water height, hydrostatic pressure
691 influences on the hydrodynamic parameters plays a major role and must be considered in
692 the model (an appromimately 5% decrease on gas hold-up per meter of depth). The
693 importance of the drag law choice is also highlighted, depending on the water quality and its
694 influence on bubble contamination.

- The gas oxygen concentration significantly depletes due to the transfer to liquid and thus the equilibrium concentration varies, which explains the difference between the mean local $<k_La>$ and global K_La coefficients. This difference becomes substantial for high soluble gas with high transfer rate and/or a high bubble column and/or low mean bubble size d_b. A depletion factor is proposed in order to warn of situations in which the experimental determination of the overall mass transfer coefficient must be conducted rigorously by considering this depletion effect through an estimation from the reoxygenation curves. The substantial impact of the depletion in the gas phase composition is drastically increasing with the length ratio H/d_b.
- The suitability of the Higbie k_L model for clean water transfer modelling is demonstrated, especially for ellipsoidal bubbles over 3 mm in full-scale aeration processes. For smaller bubbles or millimetric bubbles, mass transfer is more sensitive to water contamination and water quality remains the most important factor.
- The impact of water quality on oxygen transfer can be estimated by the contamination angle using comprehensive 1D modeling as developed in this study. This will make it possible to provide a more in-depth understanding of the impact of water quality and the main operating parameters on mass transfer in industrial tanks where the liquid phase is a complex matrix.

5. Acknowledgments

INRAE and SUEZ are gratefully acknowledged for funding this study, as are Damien Colombet and Andreia Amaral for sharing their experimental datasets.

6. References

719 Amaral A., Bellandi G., Rehman U., Neves R., Amerlinck Y., Nopens I., 2018. Towards improved accuracy in
720 modeling aeration efficiency through understanding bubble size distribution dynamics. Water research, 131,
721 346-355.
722 Baeten J.A., van Loosdrecht M., Volcke E., 2020. When and why do gradients of the gas phase composition and
723 pressure affect gas-liquid transfer? Water Research, 178,
724 Besagni G., Brazzale P., Fiocca A., Inzoli F., 2016, Estimation of bubble size distributions and shapes in two-
725 phase bubble colmun using image analysis and optical probes, Flow. Meas. Instrum., 52, 190-207
726 Capela, S., Héduit, A., Roustan, M. (2002) Influence of the water depth on fine bubble aeration efficiency in the
727 presence of surfactants. In: Proceedings of IWA 3rd World Water Congress, Melbourne, AUS, 7–12 April2002.
728 CamachoRubio F., Garcia J.L.,Molina E.,Chisti Y., 2001. Axial inhomogeneities in steady-state dissolved oxygen
729 in airlift bioreactors: predictive models. Chemical EngineeringJournal 84(1),43–55.
730 Cockx,A., Liné,A., Roustan,M., Do-Quang,Z., Lazarova,V.,1997. Numerical simulation and physical modelling of
731 the hydrodynamics in an airlift internal loop reactor.ChemicalEngineeringScience52,3787–3793.
732 Cockx, A., Do-Quang, Z., Audic, J.M., Liné, A., Roustan, M. 2001. Global and local mass transfer coefficients in
733 waste water treatment process by computational fluid dynamics. Chemical Engineering and Processing, 40 (2),
734 pp. 187-194.
735 Colombet D., Legendre D., Cockx A., Guiraud P., Risso F., Daniel C., Galinat S. 2011. Experimental study of mass
736 transfer in a dense bubble swarm. Chemical engineering science, 66, 3432-3440
737 D. Colombet, A. Cockx, P. Guiraud, D. Legendre, E. Cotton, D. Petitqueux, C. Daniel, 2013. Experiments and
738 modeling of a draft tube airlift reactor operated at high gas throughputs. Chemical Engineering Science, 104,
739 32-43
740 Colombet D., Legendre D., Risso F., Cockx A., Guiraud P., 2015. Dynamics and mass transfer of rising bubbles in
741 a homogeneous swarm at large gas volume fraction, Journal of Fluid Mechanics, 763, pp 254 – 285.
742 Dani A. 2007. Transfert de masse entre une bulle et un liquide: simulations numériques directes et fluorescence
743 induite par nappe laser. Thèse de Doctorat de l'INSA de Toulouse.
744 Dani, A., Cockx, A., Guiraud, P. 2006. Direct Numerical Simulation of Mass Transfer from Spherical Bubbles: The
745 Effect of Interface Contamination at Low Reynolds Numbers. International Journal of Chemical Reactor
746 Engineering, 4, art. no. A2, pp. 1-23.

747 Dani A., Cockx A., Legendre D., Guiraud P., 2021. Effect of spheroid bubble interface contamination on gas-
748 liquid mass transfer at intermediate Reynolds numbers: from DNS to Sherwood numbers. Chemical Engineering
749 Science, In press.
750 Dani A., Guiraud P., Cockx A., 2007. Local Measurement of Oxygen Transfer around a Single Bubble by Planar
751 Laser-Induced Fluorescence. Chemical Engineering Science, 62, 24, 7245-7252.
752 Deckwer W.D., Burckhart R., Zoll G., 1974. Mixing and Mass transfer in tall bubble columns. Chemical
753 Engineering Science, 29, 2177-2188.
754 Dhaouadi H., Poncin S., Hornut J.M., Midoux N. 2008. Gas-liquid mass transfer in bubble column reactor: an
755 analytical solution and experimental confirmation. Chem. Eng. and Processing, 47, 548-556.
756 Dijkhuizen W., Roghair I., Van Sint Annaland M., Kuiper J.A.M., 2010. DNS of gas bubble behaviour using an
757 improved 3D front tracking model – Drag force on isolated bubbles and comparison with experiments.
758 Chemical Engineering Science, 65, 1415-1426.
759 Duran Quintero C., 2015. Comportement rhéologique des boues activées : mesures, modélisation et impact sur
760 le transfert d'oxygène dans les bioréacteurs aérés. PhD thesis, Université de Toulouse, 253 p. +appendix
761 Duran C., Fayolle Y., Pechaud Y., Cockx A., Gillot S., 2016. Impact of suspended solids on the activated sludge
762 non-newtonian behavior and on oxygen transfer in a bubble column. Chemical Engineering science, 141, 154-
763 165.
764 Fayolle, Y., Gillot, S., Cockx, A., Bensimhon, L., Roustan, M., Heduit, A. 2010. In situ characterization of local
765 hydrodynamic parameters in closed-loop aeration tanks. Chemical Engineering Journal, 158 (2), pp. 207-212.
766 Fayolle Y., Cockx A., Legendre D., Gillot S. 2011. Analysis of bubble populations obtained in full-scale aeration
767 tanks in clean water. Gas liquid and gas liquid solid reactor engineering congress GLS10, 26-29 June 2011,
768 Braga, Portugal
769 Figueroa B., Legendre D., 2010. Mass or heat transfer from spheroidal gas bubbles rising through a stationary
770 liquid. Chemical Engineering Science, 65,23, 6296-6309.
771 Frössling, N., 1938. Uber die verdunstung fallenden tropfen. Gerlans Beitage Geophysik, 52,1, 170-216.
772 Gillot, S., Capela-Marsal, S., Roustan, M., Héduit, A. 2005. Predicting oxygen transfer of fine bubble diffused
773 aeration systems - Model issued from dimensional analysis. Water Research, 39 (7), pp. 1379-1387.
774 Gillot S., Héduit A., 2008. Prediction of alpha factor values for fine pore aeration systems. Water Science
775 Technology, 57,8, 1265-1269.

776 Giovannettone J.P., Gulliver J.S., 2008. Gas Transfer and Liquid Dispersion inside a deep airlift reactor. AIChE
777 Journal, 54,4, 850-861.
778 Giovannettone J.P., Tsai E., Gulliver J.S., 2009. Gas void ratio and bubble diameter inside a deep airlift reactor.
779 Chemical Engineering Journal, 149, 301-310.
780 Higbie, R., 1935. The rate of absorption of a pure gas into a still liquid during short periods of exposure.
781 Transactions AIChE Journal, 31, 365-389.
782 Jimenez, M., Dietrich, N., Grace, J.R., Hébrard, G. 2014. Oxygen mass transfer and hydrodynamic behaviour in
783 wastewater: Determination of local impact of surfactants by visualization techniques. Water Research, 58, pp.
784 111-121.
785 Longo, S., d'Antoni, B.M., Bongards, M., Chaparro, A., Cronrath, A., Fatone, F., Lema, J.M., Mauricio-Iglesias, M.,
786 Soares, A., Hospido, A. 2016. Monitoring and diagnosis of energy consumption in wastewater treatment plants.
787 A state of the art and proposals for improvement. Applied Energy, 179, pp. 1251-1268.
788 Loubière K., Hébrard G., Guiraud P., 2003. Dynamics of bubble growth and detachment from rigid and flexible
789 orifices. The Canadian Journal of Chemical Engineering, 81,3-4, 499-507.
790 Manjrekar O.N., 2016. Hydrodynamics and Mass Transfer in Bubble Columns. Engineering and Applied Sciences
791 Theses and Dissertations, 160.
792 Mudde R.F., Hartevel W.K., van den Akker H.E.A., 2009, Uniform flow in bubble columns, Ind. Eng. Chem. Res.,
793 48, 148-156.
794 Pöpel H.J., Wagner M., 1994. Modelling of Oxygen Transfer in Deep Diffused-Aeration Tanks and Comparison
795 with Full-Scale Plant Data. Wat. Sci. Tech., 30, 4, 71-80.
796 Rosso D., Stenstrom M. K., 2005. Economic Implications of Fine Pore Diffuser Aging. Proc. Water Environ. Fed.,
797 78, 810-815.
798 Rosso D., Huo D.L., Stenstrom M. K., 2006. Effects of interfacial surfactant contamination on bubble gas
799 transfer. Chemical Engineering Science, 61, 5500-5514.
800 Roustan, M. 1996. Quels sont les critères d'extrapolation pour les systèmes d'aération? Tribune de l'Eau, 1, pp.
801 53-58.
802 Rubio F., Garcia J., Molina E., Chisti Y., 1999. Steady-state axial profiles of dissolved oxygen in tall bubble
803 column bioreactors. Chemical Engineering Science, 54, 1711-1723.

804 Sadhal S.S., Johnson R.E., 1983. Stokes Flow Past Bubbles and Drops Partially Coated with Thin Films. Part I.
805 Stagnant Cap of Surfactant Film – Exact Solution. J. Fluid Mech., 126 , 237-250.
806 Sardeing R., Painmanakul P., Hébrard G., 2006. Effect of surfactants on liquid-side mass transfer coefficients in
807 gas-liquid systems : A first step to modeling. Chemical Engineering Science, 61, 6249-6260.
808 Schiller L., Naumann Z., 1938. A drag coefficient correlation. Z Ver Deutsch Ing., 77-318
809 Shah Y.T., Kelkar B.G., Godbole S.P., 1982. Design Parameters Estimations for Bubble Column Reactors. AIChE
810 Journal, 28,3, 353-379.
811 Takemura F., Yabe A., 1999. Rising Speed and Dissolution Rate of a Carbon Dioxide Bubble in Slightly
812 Contaminated Water. J. Fluid Mech., 378, 319-334.
813 Talvy S., Cockx A., Liné A., 2007a. Modeling of oxygen mass transfer in a gas-liquid airlift reactor. AIChe Journal,
814 53, 2, 316-326.
815 Talvy S., Cockx A., Liné A., 2007b. Modeling hydrodynamics of gas-liquid airlift reactor. AIChe Journal, 53, 2,
816 335-353.
817 Talvy, S., Cockx, A., Line, A. 2005. Global modelling of a gas-liquid-solid airlift reactor. Chemical Engineering
818 Science, 60 (22), pp. 5991-6003.
819 Tomiyama A., Kataoka I., Zun I., Sakaguchi T., 1998. Drag coefficients of single bubbles under normal and micro
820 gravity conditions. JSME International Journal, 41, 2.
821 Vitankar, V.S.,Joshi,J.B., 2002. A comprehensive one-dimensional model for prediction of flow pattern in bubble
822 columns. Chemical Engineering Research and Design 80 (5),499–512.
823 Wallis, G.B., 1961. Some hydrodynamic aspects of two-phase flow and boiling. Int. Heat Transfer Conference,
824 Boulder, Colorado USA, 2, 319-325.
825 Wallis,G.B.,1969. One Dimensional Two-phase Flow. Mcgraw Hill.
826 Xu F., Cockx A., Hébrard G., Dietrich N., 2018. Mass transfer and diffusion of a single bubble rising in polymer
827 solutions. Ind. Eng. Chem. Re., 57, 15181-15194.
828 Zlokarnik, M. 1979. Sorption characteristics of slot injectors and their dependency on the coalescence
829 behaviour of the system. Chemical Engineering Science, 34 (10), pp. 1265-1271.
830 Zlokarnik M., 2005. Sorption characteristics for gas-liquid contacting in mixing vessels. Advances in Biochemical
831 Engineering, 8, 133-151.

832 Zuber N., Findlay J.A., 1965. Average volumetric concentration in two phase systems. Trans. ASME. J. of Heat
833 Transfer, 87-453.

Input data

- Physico-chemical parameters
- Column height
- Gas superficial velocity j_G
- Bubble diameter d_B

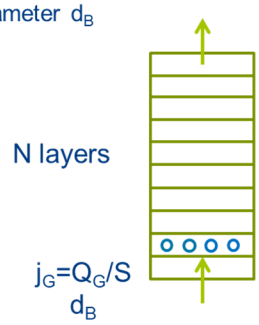

Hydrodynamic calculation (steady state/input for mass transfer)

- Gas hold-up ε_G
- Slip velocity/gas velocity
- Hydrostatic pressure
- Bubble diameter variation

Mass transfer (dynamic)

- C_L = f(t) (perfectly mixed liquid)
- C_G = f(t) for each height z